

# Design and material evaluation for a novel lumbar disc replacement implanted via unilateral transforaminal approach

Gonzalez Alvarez, Alba; Dearn, Karl; Shepherd, Duncan

DOI:

[10.1016/j.jmbbm.2018.12.011](https://doi.org/10.1016/j.jmbbm.2018.12.011)

License:

Creative Commons: Attribution-NonCommercial-NoDerivs (CC BY-NC-ND)

Document Version

Peer reviewed version

Citation for published version (Harvard):

Gonzalez Alvarez, A, Dearn, K & Shepherd, D 2019, 'Design and material evaluation for a novel lumbar disc replacement implanted via unilateral transforaminal approach', *Journal of the Mechanical Behavior of Biomedical Materials*, vol. 91, pp. 383-390. <https://doi.org/10.1016/j.jmbbm.2018.12.011>

[Link to publication on Research at Birmingham portal](#)

## Publisher Rights Statement:

Checked for eligibility: 18/12/2018

## General rights

Unless a licence is specified above, all rights (including copyright and moral rights) in this document are retained by the authors and/or the copyright holders. The express permission of the copyright holder must be obtained for any use of this material other than for purposes permitted by law.

- Users may freely distribute the URL that is used to identify this publication.
- Users may download and/or print one copy of the publication from the University of Birmingham research portal for the purpose of private study or non-commercial research.
- User may use extracts from the document in line with the concept of 'fair dealing' under the Copyright, Designs and Patents Act 1988 (?)
- Users may not further distribute the material nor use it for the purposes of commercial gain.

Where a licence is displayed above, please note the terms and conditions of the licence govern your use of this document.

When citing, please reference the published version.

## Take down policy

While the University of Birmingham exercises care and attention in making items available there are rare occasions when an item has been uploaded in error or has been deemed to be commercially or otherwise sensitive.

If you believe that this is the case for this document, please contact [UBIRA@lists.bham.ac.uk](mailto:UBIRA@lists.bham.ac.uk) providing details and we will remove access to the work immediately and investigate.

# DESIGN AND MATERIAL EVALUATION FOR A NOVEL LUMBAR DISC REPLACEMENT IMPLANTED VIA UNILATERAL TRANSFORAMINAL APPROACH

## Author names and affiliations

Alba Gonzalez Alvarez, *Department of Mechanical Engineering, School of Engineering, University of Birmingham*

Karl D. Dearn, *Department of Mechanical Engineering, School of Engineering, University of Birmingham*

Duncan E.T. Shepherd, *Department of Mechanical Engineering, School of Engineering, University of Birmingham*

**Corresponding author:** Alba Gonzalez Alvarez

[Ms.alba.gonzalez@gmail.com](mailto:Ms.alba.gonzalez@gmail.com)

*Mechanical Engineering department*

*University of Birmingham*

*B152TT Birmingham*

## Abstract

The degeneration of the intervertebral disc is one of the principal causes of low back pain. Total disc replacement is a surgical treatment that aims to replace the degenerated disc with a dynamic implant to restore spine biomechanics. This paper proposes the first design of an elastomeric lumbar disc replacement that is implanted as a pair of devices via unilateral transforaminal surgical approach. Furthermore, several biomaterials (Polyurethanes (PU) and Polycarbonate Urethanes (PCU)) are evaluated for the purpose of the implant to mimic the axial compliance of the spine. Bionate II 80A (a pure PCU), Elast Eon 82A E5-325 (a PU with polydimethylsiloxane and polyhexamethylene oxide), Chronosil (a PCU based silicone elastomer) 80A with 5% and 10% of silicone were obtained and injection moulded according to the shape of the implant core, which was defined after a stress distribution analysis with the finite element method. The dimensions for each specimen were: 14.6 x 5.6 x 6.1 mm (length, width and height). Quasistatic compression tests were performed at a displacement rate of 0.02 mm/s. The obtained stiffness for each material at 1 mm displacement was: Bionate II 80A, 448.48 N/mm; Elast Eon 82A E5-325, 216.55 N/mm; Chronosil 80A 5%, 127.73 N/mm; and Chronosil 80A 10%, 126.48 N/mm. Dimensional changes were quantified after two quasi-static compression tests. Plastic deformation was perceived in all cases with a total percentage of height loss of:  $4.1 \pm 0.5\%$  for Elast Eon 82A E5-325;  $3.2 \pm 0.5\%$  for Chronosil 80A 10%;  $2.7 \pm 0.3\%$  for Chronosil 80A 5% and  $1.1 \pm 0.2\%$  for Bionate II 80A. The mechanical behavior of these biomaterials is discussed to assess their suitability for the novel disc replacement device proposed.

## Keywords

Polyurethane biomaterials; polycarbonate urethane biomaterials, stiffness; deformation; elastomeric lumbar disc replacement;

## 1. INTRODUCTION

Low back pain (LBP) is a worldwide burden experienced by 80% of the population at least once in their lifetime (Baliga et al., 2015). One of the principal causes of LBP is the degeneration of spinal structures like the Intervertebral Disc (IVD) (Salzman et al., 2017). Spinal fusion is a surgical option for the treatment for Degenerative Disc Disease (DDD) and consists of eradicating the source of pain by eliminating motion of the damaged spinal segment with implanted instrumentation. Total Disc Replacement (TDR) is an alternative treatment that aims to preserve spinal mobility by removing the damaged IVD and replacing it with a dynamic device. The better performance of TDR in comparison with fusion remains unclear (Salzman et al., 2017; Rao and Cao, 2014) due to many marketed devices having caused numerous complications. A common problem is the alteration of the biomechanics of the spinal segment treated leading to degeneration of other spinal structures (Abi-Hanna et al., 2017). This complication may be avoided by providing a more physiological range of motion that includes axial compliance with the incorporation of an elastomeric component (Vicars et al., 2017). Elastomeric devices are demonstrating a better physiological range of motion in comparison to ball and socket devices because they replicate the viscoelasticity of the natural disc (Vicar et al. 2017).

Another drawback hampering the use of TDR treatment is the anterior approach undertaken when surgeons implant the devices (Salzmann et al., 2017). This surgical procedure requires well-trained surgeons as it presents a risk with respect to vascular structures around the spine (Vital and Boissiere, 2014). None of the existing TDR devices on the market are implanted via the transforaminal approach, a widely applied surgical technique for spinal fusion that has shown favourable outcomes and advantages (such as less time of postoperative recovery) in comparison with posterior and anterior approaches (Deng et al., 2016; Zhang et al., 2014).

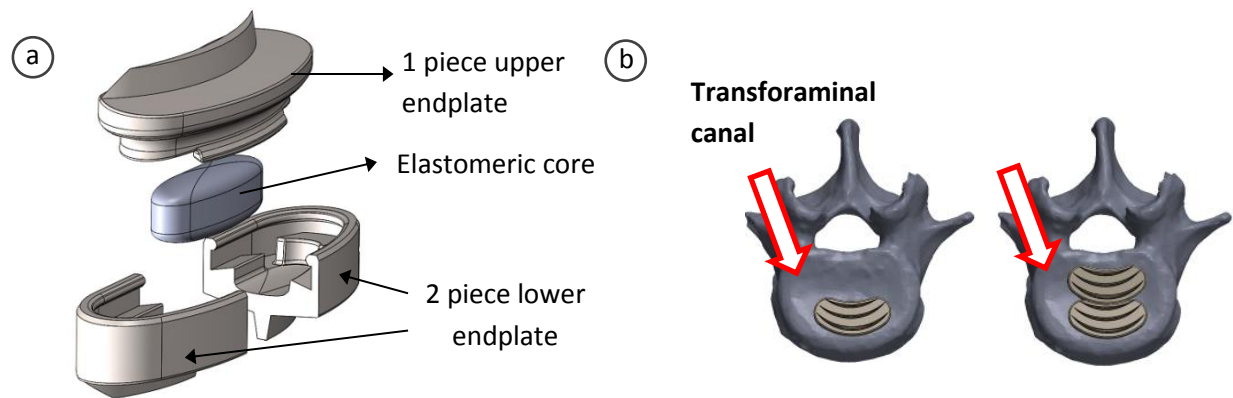
This paper describes a novel design for a lumbar disc replacement inserted as a pair of implants via an unilateral transforaminal approach and investigates the mechanical feasibility and the material selection for the device. The implant includes an elastomeric core in between two metallic endplates to mimic the viscoelastic behaviour of a healthy disc. The finite element (FE) method was used to verify that the endplates provided enough strength to prevent any plastic deformation during simulated spinal loading. Then, the elastomeric core was dimensioned and further investigated in order to find a suitable material that most closely reproduced the stiffness of the lumbar spine.

Polyurethanes (PUs) and Polycarbonate Urethanes (PCUs) represent two important classes of polymers used in a broad range of biomedical applications. Motion preservation of the spine is one

of their uses because of the elastomeric nature of the collagen and fluids that constitute the IVD (John, 2014). Therefore, four long-term implantable PU and PCUs with and without silicone additives were obtained and mechanically evaluated to assess their suitability for the device purposes.

## 2. DESCRIPTION OF A NOVEL DEVICE

The novel device is an elastomeric 4-piece device (figure 1a) designed to be inserted as a pair, one implant after the other (figure 1b) by way of unilateral transforaminal approach. The implant includes an elastomeric core enclosed in between two metallic retaining plates made from Cobalt Chromium (CoCr) alloy. CoCr was chosen because it provides greater strength and resistance to fatigue in comparison to titanium alloy (Han et al., 2017) to better resist the fatigue loads of the lumbar spine. The material for the elastomeric core will be investigated in this paper. A central keel in both endplates allows device fixation to the vertebrae during implantation.



*Figure 1: Novel design of the device. a) Exploded view of a single device. b) Surgical technique consisting of the insertion of two devices, one after the other, via unilateral transforaminal approach. The insertion direction is highlighted with arrows.*

The upper endplate articulates with the core and comes into contact with the lower endplate when a maximum range of motion has been achieved (figure 2). The assembly has been designed to provide a similar physiological motion to the L4/L5 lumbar spinal segment because it is the most common segment that causes spinal instability (Park, 2015; Okoro and Sell, 2010). The range of motion provided is: 4° in flexion, 2° in extension, 2° in lateral bending for each side and 2° in axial rotation. The device also allows axial compression providing 6 degrees of freedom. The centre of rotation can vary during motion, compensating for small errors in device placement (Salzmann et al., 2017). The assembly is also designed to maintain the height of the device at 10 mm (intervertebral lumbar height suggested by ASTM F2346-05 (2011)), even in the case of core failure (height loss due to plastic deformation, fracture, etc.).

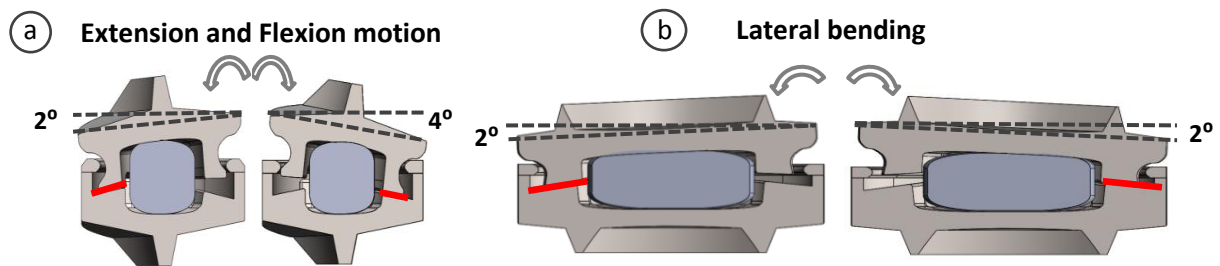


Figure 2: Examples of the maximum range of motion delivered by one device. Maximum motion is achieved when the contact between the endplates occurs, marked with red lines at each range. a) Maximum extension and flexion motion. b) Maximum lateral bending motion.

The size of the device is limited by the canal of insertion for the transforaminal approach which anatomically allows a maximum implant width of 10 mm (Soriano-Baron et al., 2015). Three sizes (S, M and L) are provided to accommodate to different spinal segments and patient anatomies. Lengths and heights (in mm) for sizes S, M and L are: 28 and 10; 30 and 12; and 32 and 14, respectively.

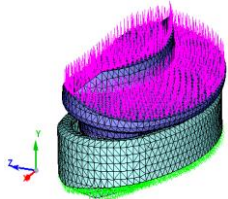
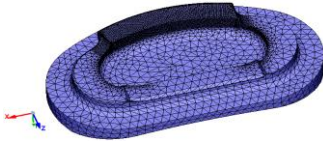
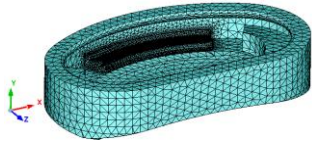
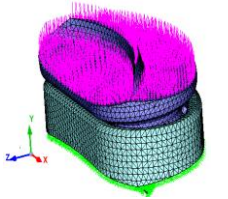

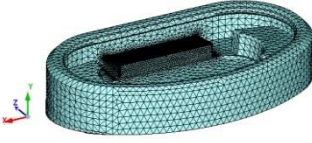
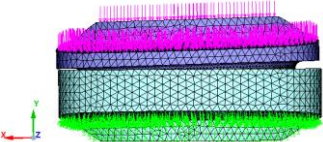
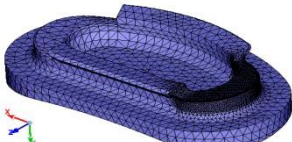
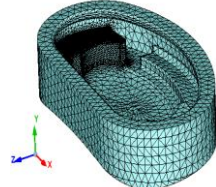
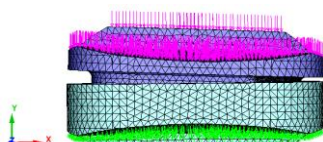

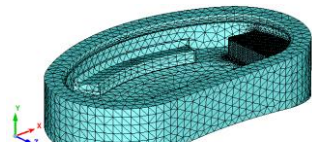
### 3. SIZING OF THE IMPLANT CORE

#### 3.1. Finite element analysis models

In order to dimension the elastomeric core to select a suitable material, a stress distribution analysis of the metallic endplates was performed with finite element analysis (FEA) to verify that these components met strength requirements under simulated spinal loading. The thicknesses of the walls for the upper and lower endplates that contacted each other during maximum range of motion were the design features to be minimized so that they maximised the space for the elastomeric core whilst avoiding plastic deformation within the endplates. Four scenarios were studied when the endplates came into contact to restrict motion during maximum range of motion allowance: “model 1”: when the device provides 6° of flexion; “model 2” for 4° in extension, “model 3” and “model 4” for 2° of each lateral bending positions. The smallest implant (size S) was selected for the analysis as it represented the smallest geometry. The four models were prepared in Solidworks 2014 (Dassault Systemes SolidWorks Corporation, Waltham, MA) and then transferred to Simlab 14.2 (Altair Engineering, Troy, Michigan, USA) to generate the FE models. Mesh controls and mesh refinements were assigned at the contact surfaces between the endplates where high stresses were expected. A general element size of 1 mm was used for all the FE models except for the meshing refinements that had an element size of 0.2 mm. Second order tetrahedral elements were used for the mesh. The parts were modelled as CoCr alloy, an isotropic, homogeneous and linearly elastic material with an elastic Young’s modulus of 210 GPa and a Poisson’s ratio of 0.30 (Klues et al., 2010). The bottom

surface of the lower endplate was fully constrained to mimic anchorage to the lower vertebra. A compressive static load of 1500 N was applied to each model on the top surface of the upper endplate, assuming uniform load distribution. This loading condition was determined on the basis that two devices are inserted per surgery and the maximum compressive lumbar loads have been reported to be up to 2000 N (British Standard Institution, 2011). Therefore, a safety coefficient of 1.5 was applied. Contact zones were defined for the upper and lower endplate at their contact areas for the different scenarios analysed with a stick contact. The volume mesh characteristics of each component for the four positions analysed with the number of tetra elements generated can be seen in table 1.

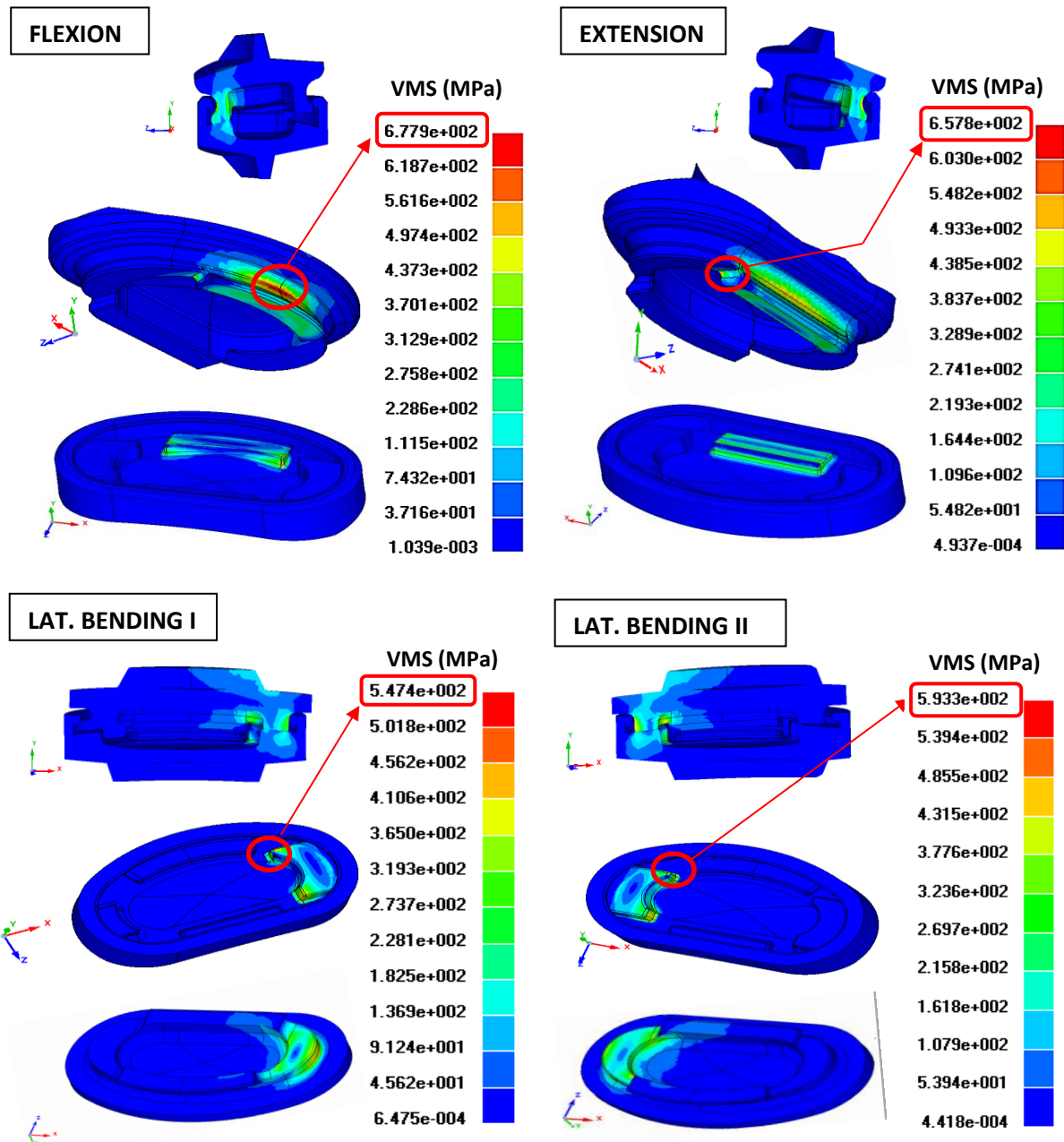
**Table 1-** FE models of the device: Model 1 (flexion), Model 2 (extension), Model 3 (Lateral bending I) and Model 4 (Lateral bending II); purple arrows represent the compressive loads applied to the upper endplate; green arrows represent the fully constraint points that simulate anchorage of the lower endplate to the vertebra. The mesh refinements in each plate can be seen at the contact surface with the other plate for each model.

RANGE OF MOTION ANALYSED	NUMBER OF 10-NODE TETRAHEDRAL ELEMENTS		
	Assembly model	Upper plate	Lower plate
<b>Model 1 : FLEXION</b>	 <b>34091</b>	 <b>15256</b>	 <b>18835</b>
<b>Model 2 : EXTENSION</b>	 <b>34366</b>	 <b>17834</b>	 <b>16532</b>
<b>Model 3 : LAT. BENDING I</b>	 <b>29787</b>	 <b>14652</b>	 <b>15135</b>
<b>Model 4 : LAT. BENDING II</b>	 <b>31175</b>	 <b>15321</b>	 <b>15854</b>



### 3.2. Results

Results (figure 3) demonstrated that the maximum von Mises Stress (VMS) value was 678 MPa and occurred in the upper endplate during flexion. The maximum stress for the extension motion was 658 MPa with the maximum value located in the upper endplate as well. During lateral bending I, the maximum VMS (547 MPa) was placed on the lower endplate at the contact surface with the upper endplate. For the lateral bending II the maximum VMS was located in the symmetrical part with a maximum stress value of 593 MPa.



**Figure 3-** Results of the von Mises Stress (VMS) distribution of the four models analysed: flexion, extension, lateral bending I and lateral bending II. Values of stress are expressed in MPa. The maximum VMS value for each material is marked with a red circle.

None of these stress values reached the yield strength (841 MPa) or fatigue strength (725 MPa) of the CoCr alloy (Yao et al., 2011) and, therefore, the design was considered to be safe both under static and fatigue compressive loads in the four cases analysed. The implant strength requirement was found to be met in all cases.

#### **4. MECHANICAL TESTING OF BIOMATERIALS FOR THE IMPLANT CORE**

With the endplates meeting the strength requirements, the space for the elastomeric core was validated and the part dimensioned. The aim of this section was to find an appropriate material for the core that provided similar stiffness to the lumbar spine. Suitability was determined by obtaining the stiffness of several long term biomaterials by using mechanical testing and directly comparing them with the corresponding stiffness of a representative functional spinal unit (FSU) of the lumbar region for forces in compression reported from literature.

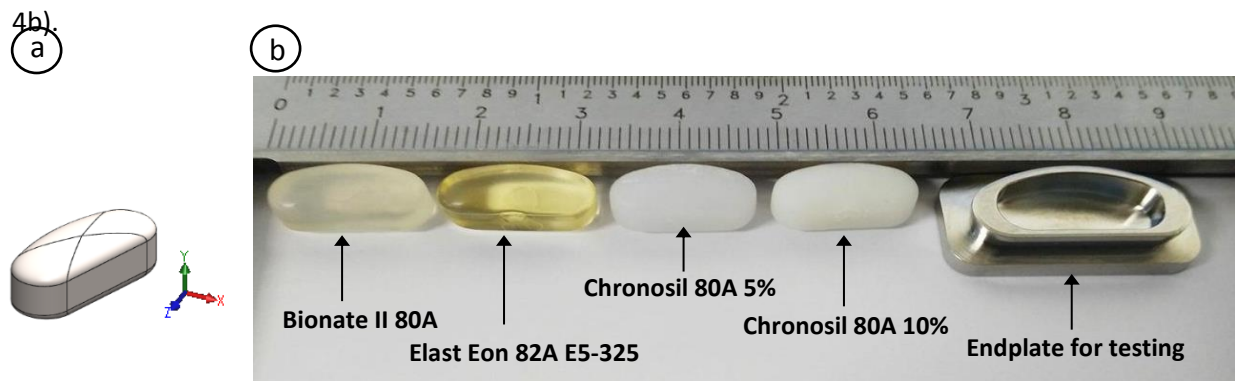
##### **4.1. Materials and methods**

Material selection for testing was carried out following a comprehensive market research of PUs and PCUs used in biomedical applications and a wide range of compositions were finally chosen for evaluation, including carbonate and silicone groups. The carbonate group of the PCUs provides polymers with high-pressure resistance and tensile strength, properties that closely match the lumbar disc mechanics and the incorporation of silicone has been shown to provide oxidative stability (Gunatillake and Aghikari, 2016; Ward and Jones, 2011). Consequently, the four materials chosen for assessment were:

- Bionate II 80A (DSM Corporate, Heerlen, Netherlands), a PCU elastomer used in various spinal devices on the market such as the LP-ESP lumbar disc replacement (FH Orthopedics, Chicago, IL, USA) (Lazennec et al., 2013) or the BDyn dynamic posterior stabilization device (S14 Implants, Pessac, France) (Lawless et al., 2016).
- Chronosil 80A (AdvanSource Biomaterials, Wilmington, Massachusetts, United States) a polycarbonate based silicone elastomer. Chronosil is a well-known material for intravascular applications with resistant to environmental stress cracking and, consequently, suitable for long-term applications (Francolini and Piozzi, 2016). Two different percentages of silicone were selected for evaluation: Chronosil 80A 5% and Chronosil 80A 10%.
- Quadrasil Elast-Eon 82A E5-325 (Aortech International PLC, Weybridge, United Kingdom) a PU with polydimethylsiloxane and polyhexamethylene oxide. Elast Eon has been reported to be a very biostable material (Gunatillake and Adhikari, 2016).



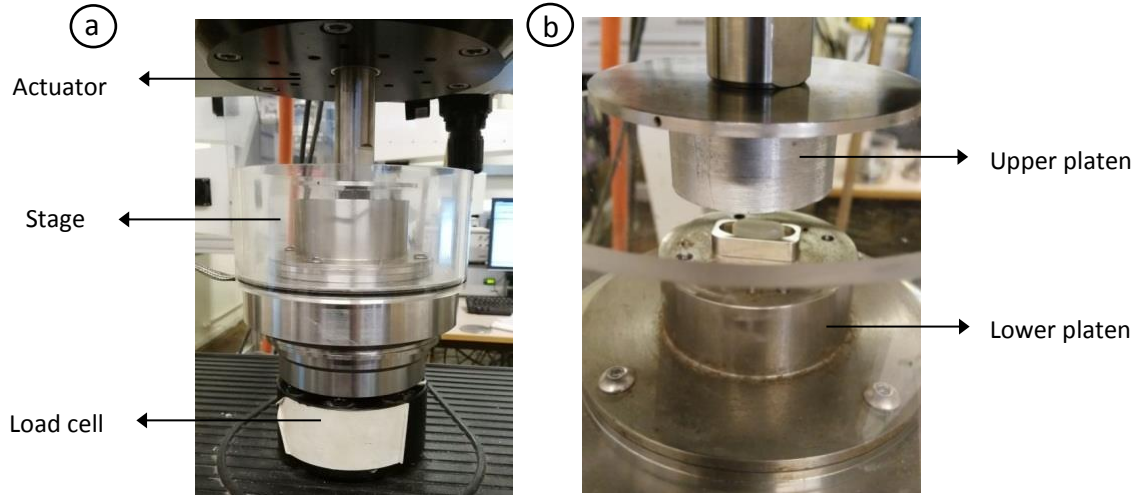
The four materials were obtained and injection moulded (Statice, Besançon, France), according to the core design (figure 4a and b). The dimensions for each specimen were: 14.6 x 6 x 6.35 mm (length in “z” axis, width in “x” direction and height in “y” from figure 4a). A stainless steel lower endplate was manufactured (Statice, Besançon, France) with a simplified geometry in order to have a curved surface where the samples could be placed against during the compression testing (figure



**Figure 4-** Elastomeric core. a) Specimen 3 dimensional computer-aided design model with datum. b) Manufactured specimens of the four materials evaluated and the endplate for testing.

Seven samples of each material were tested in quasi-static compression to obtain force-displacement curves. The displacement rate was set at 0.02 mm/s. A single specimen was compressed in each test. The axial compressive stiffness for the natural IVD has been reported to be in the range from 1700 to 3000 N/mm (Virgin, 1951; Gardner-Morse and Stokes, 2004; Bouzakis et al., 2004; Kemper et al., 2007). The LP-ESP lumbar disc replacement stated a value of 2300 N/mm (Lazennec et al., 2013) whereas White and Panjabi (1990) described a value of 2000 N/mm for the L4/L5 as a FSU. As the surgical implantation proposed in this study required the use of a pair of implants, the target stiffness for each specimen was established as a minimum of 1000 N/mm.

The machine used for the compression testing was a Bose ElectroForce 3300 Series II Test Instrument (Bose Corporation, ElectroForce Systems Group, Eden Prairie, Minnesota, USA) using Win Test 4.1 software. The mechanical testing set up is shown in figure 5.



**Figure 5-** Mechanical testing using the Bose Electroforce 3300 machine. a) Detailed view of the actuator, the stage and the load cell. b) View of the specimen inside the endplate before compression from the upper platen.

The maximum displacement was limited to 2.3 mm. This limit was imposed to avoid actuator/endplate contact. In order to investigate the potential change in the force vs. displacement curves after a first deformation (Test 1), a second test was performed 24 hours later (Test 2); the change in the force vs. displacement curves from Test 2 was directly compared to the initial Test 1. This provided information about the change of the material after a high compressive force.

The geometrical changes in the specimens after the compressive forces were also analysed as the device performance and design is dependent on the deformation of the elastomeric core. Changes in height were relevant due to the range of motion delivery of the device. Variations in length and weight provided information about the required clearances between the core and the endplates to allow the core to bulge without constraints under compression. Measurements were taken with a digital Vernier calliper with an accuracy of 0.02 mm. Three measurements were taken for each dimension and the average was calculated. The parameters of interest were height, length and width of each specimen before and after Test 1, 24 hours later (before Test 2) and after Test 2. Values were compared for each material to analyse deformation.

## 4.2. Results

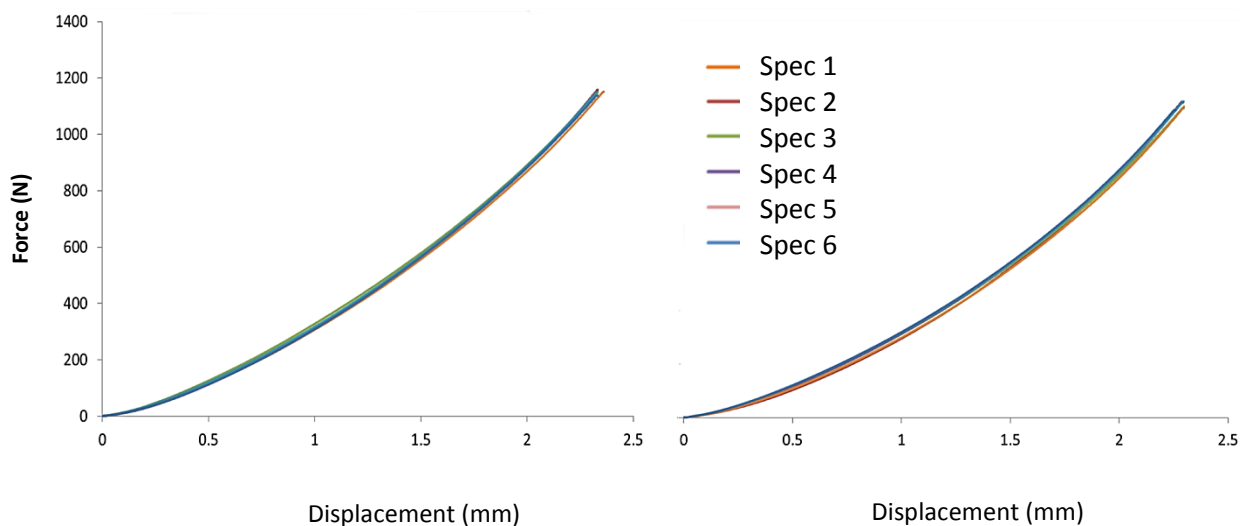
### 4.2.1. Force vs Displacement curves

Table 2 shows the mean values of force with standard deviations for each material at 0.5, 1, 1.5 and 2 mm of displacement for Test 1 and Test 2. All the tests achieved the 2.3 mm of maximum displacement, which was equivalent to 36.2% of the specimen height. Figures 6 and 7 show an

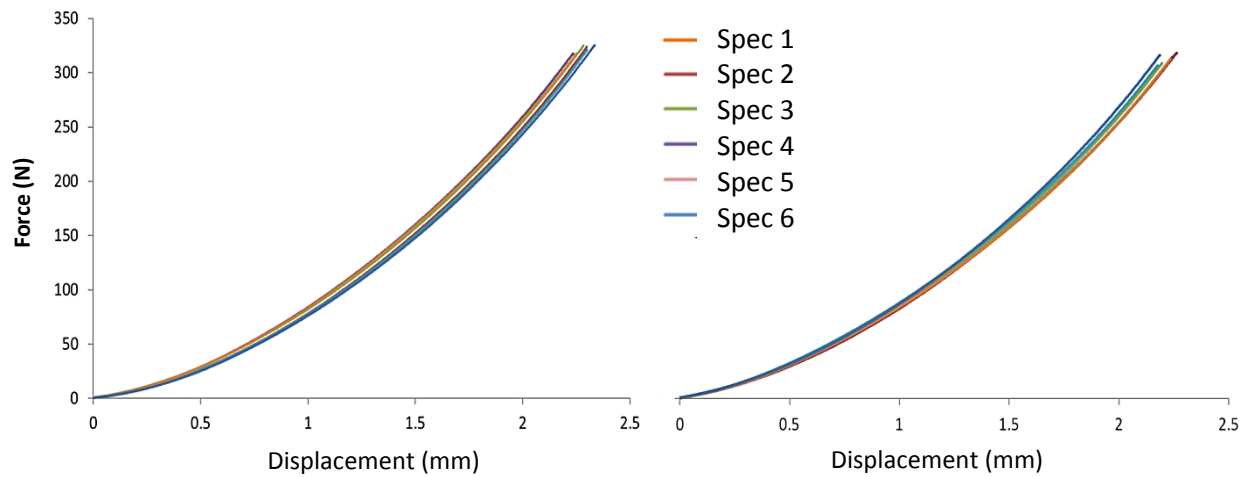
example of the force against displacement curves for the stiffest and least stiff materials (Bionate II 80 A and Chronosil 80 A 10%, respectively) for Test 1 (left) and Test 2 (right).

**Table 2-** Mean values of forces with standard deviations for each material at 0.5, 1, 1.5 and 2 mm of displacement for Test 1 and Test 2.

Displ. (mm)	MEAN FORCE (N) IN TEST 1				MEAN FORCE (N) IN TEST 2			
	Bionate	Elast-Eon	Chronosil 5%	Chronosil 10%	Bionate	Elast-Eon	Chronosil 5%	Chronosil 10%
0.5	117.4 ± 5.6	53.6 ± 2.4	27.2 ± 2.2	27.7 ± 1.6	115.9 ± 7.2	54.6 ± 4.2	25.4 ± 2.0	31.8 ± 1.0
1	313.5 ± 7.5	151.7 ± 4.0	79.8 ± 5.8	78.3 ± 3.4	310.9 ± 10.2	149.8 ± 8.0	74.9 ± 5.4	86.5 ± 2.0
1.5	566.6 ± 7.8	274.8 ± 6.1	154.6 ± 9.9	154.7 ± 5.2	570.5 ± 10.0	266.7 ± 10.3	147.6 ± 9.6	162.0 ± 3.4
2	883.7 ± 7.9	422.3 ± 9.8	252.5 ± 14.4	256.3 ± 6.3	916.4 ± 11.5	411.8 ± 11.3	249.2 ± 14.7	262.0 ± 5.9



**Figure 6-** Force vs. displacement curves of Bionate II 80 A specimens (Spec) for Test 1 (left) and Test 2 (right). Spec= specimen.



**Figure 7-** Force vs displacement curves of Chronosil 80 A 10% specimens (Spec) for Test 1 (left) and Test 2 (right). Spec= specimen.

The behaviour of the four materials was nonlinear. A second-order polynomial trendline fitted to the results and can be seen in table 3.

**Table 3-** Fits for the force vs. displacement curves of the four materials tested.

	Fits for the force-displacement curves
<b>Bionate II 80A</b>	$F = 129 x^2 + 190.48 x - 9.2303$ ; $R^2 = 0.9999$
<b>Elast Eon 82A E5-325</b>	$F = 56.695 x^2 + 103.16 x + 9.1766$ ; $R^2 = 0.9998$
<b>Chronosil 80A 10%</b>	$F = 46.266 x^2 + 33.948 x - 0.4184$ ; $R^2 = 1$
<b>Chronosil 80A 5%</b>	$F = 50.301 x^2 + 27.132 x + 0.8385$ ; $R^2 = 0.9999$

#### 4.2.2. Mean stiffness

The stiffness for each material “k” was calculated as the derivative of the polynomial equations ( $k=dF/dx$ ) at 1 mm of displacement (table 4).

**Table 4-** Stiffness “k” (N/mm) of each material and the target stiffness at 1 mm of displacement.

	<b>Bionate II 80A</b>	<b>Elast Eon 82A E5-325</b>	<b>Chronosil 80A 5%</b>	<b>Chronosil 80A 10%</b>	<b>Target stiffness</b>
Stiffness “k” (N/mm)	448.48	216.55	127.73	126.48	1000

The stiffest material was Bionate (448.48 N/mm) followed by Elast Eon (216.55 N/mm), Chronosil 5% (127.73 N/mm) and Chronosil 10% (126.48 N/mm). None of them achieved the minimum target stiffness of 1000 N/mm to mimic the axial compliance of the intervertebral disc.

### 4.2.3. Deformation

Table 5 shows the average percentage of deformation in height (H), length (L) and width (W) for each material after Test 1 (% Deformation Test 1), between Test 1 and Test 2 (% Recovery after 24 hours), after Test 2 (% Deformation Test 2) and the total deformation after Test 2 in comparison with the original dimensions of the specimens after manufacturing (% total def.). Note, (-) expresses a reduction and (+) an increase in the correspondent dimension.

**Table 5-** Average percentages of deformations for each material after Test 1, recovery after 24 hours, after Test 2 and total deformation with standard deviations. Def= deformation. H= height. L= length. W= width.

		% Def after Test 1	% recovery after 24h	% Def. after Test 2	% Total Def.
<b>Bionate II 80A</b>	H	(-) 1.0 ± 0.3	(+) 0.4 ± 0.1	(-) 0.5 ± 0.1	(-) 1.1 ± 0.2
	L	(+) 0.4 ± 0.1	(-) 0.1 ± 0.0	(+) 0.4 ± 0.1	(+) 0.7 ± 0.1
	W	(+) 0.8 ± 0.2	(-) 0.4 ± 0.1	(+) 0.5 ± 0.3	(+) 0.9 ± 0.2
<b>Elast Eon 82A E5-325</b>	H	(-) 3.6 ± 0.6	(+) 3.3 ± 0.4	(-) 3.7 ± 0.6	(-) 4.1 ± 0.5
	L	(+) 0.9 ± 0.3	(-) 0.5 ± 0.2	(+) 0.4 ± 0.1	(+) 0.8 ± 0.2
	W	(+) 3.1 ± 0.4	(-) 2.2 ± 0.3	(+) 2.2 ± 0.4	(+) 3.0 ± 0.5
<b>Chronosil 80A 5%</b>	H	(-) 2.2 ± 0.4	(+) 1.5 ± 0.3	(-) 2.0 ± 0.4	(-) 2.7 ± 0.3
	L	(+) 0.5 ± 0.1	(-) 0.2 ± 0.0	(+) 0.3 ± 0.1	(+) 0.7 ± 0.1
	W	(+) 1.8 ± 0.3	(-) 1.2 ± 0.2	(-) 1.8 ± 0.3	(+) 2.4 ± 0.2
<b>Chronosil 80A 10%</b>	H	(-) 2.7 ± 0.5	(+) 1.9 ± 0.2	(-) 2.4 ± 0.5	(-) 3.2 ± 0.5
	L	(+) 0.7 ± 0.2	(-) 0.3 ± 0.0	(+) 0.4 ± 0.1	(+) 0.8 ± 0.2
	W	(+) 2.3 ± 0.4	(-) 1.2 ± 0.3	(+) 2.2 ± 0.4	(+) 2.5 ± 0.3

Results of the four materials showed that all the specimens deformed plastically after the first and second quasi-static compression tests. The height was the dimension that changed the most in all cases, followed by width and length. Each compression (Test 1 and Test 2) caused a reduction of height as well as an increase in length and width in all cases. Recovery time affected these parameters in the opposite way. Elast Eon 82A E5-325 was the most deformable material followed by Chronosil 80A 10%, Chronosil 80A 5% and Bionate II 80A, respectively.

## 5. DISCUSSION

This paper has investigated the first elastomeric lumbar disc replacement that is inserted via unilateral transforaminal approach as a pair of devices. The anatomical feasibility of inserting two

nested curved implants via this approach has been confirmed in previous studies for the treatment of spinal fusion (Soriano-Baron et al., 2015). However, this procedure has never been applied for the insertion of dynamic implants to restore spine biomechanics.

A preliminary stress distribution analysis was performed with FEA to verify that the metallic parts met strength requirements under simulated spinal loading whilst guaranteeing a safety coefficient of 1.5. The endplates were analysed during delivery of maximum range of motion in flexion, extension and both lateral bending motions. The maximum VMS obtained in those four scenarios was: 678 MPa, 659 MPa, 547 MPa and 593 MPa, respectively, lower values than the yield (841 MPa) and fatigue (725 MPa) strength of CoCr alloy (Yao et al., 2011). This analysis helped verified the dimensions for the endplates so that the size for the elastomeric core could be defined accordingly.

Mechanical evaluation of several long term biomaterials was completed to assess their suitability for the elastomeric core of the device proposed. Quasi-static compression tests were carried out to obtain the compression stiffness of the materials due to this information not being provided by the suppliers. The core specimens were tested inside a lower endplate that presented the same curvature of the device lower endplate so that the compression mechanism of the actual device was accurately replicated in the test. The elastomer bulging was realistic and was not constrained by the lateral walls of the lower endplate, replicating what would occur in the actual device. Only compression loading was analysed since it is the major form of load that the IVD is subjected to (Inoue and Orias, 2011). The main differences between the compression mechanism of the testing and the actual device were: (1) the upper platen that compressed the core specimens was flat whereas the upper endplate of the device design is slightly curved; (2) the testing was performed only with one core specimen whereas the implant was designed to work as a pair. Therefore, half of the total target stiffness pursued for the pair of devices was aimed for each single core specimen: 1000 N/mm.

Results of the quasi-static tests showed that the average stiffness for each material at 1 mm of displacement was: 448.48 N/mm for Bionate II 80A; 216.55 N/mm for Elast Eon E5-325; 127.73 N/mm for Chronosil 80A 5% and 126.48 N/mm for Chronosil 80A 10%. Bionate II 80A was the stiffest material. This may be due to the carbonate segment in its composition combined with the lack of silicone that would weaken its strength. It also presented a stiffer behaviour in Test 2 after 1.5 mm of displacement. Elast Eon 82A E5-325 showed 51.7% lower average stiffness than Bionate at 1 mm of displacement. This may be due to its high elasticity and the lack of a polycarbonate chain in its composition, being only 32.5% of the material hard segment content (Osman et al., 2011). Elast Eon presented a very similar trendline of force against displacement for Test 1 and Test 2 while reaching

lower forces in the second test. Samples of Chronosil 80A, both with 5% and 10% of silicone, presented similar curve tendencies despite their different compositions in silicone. The average stiffness values for Chronosil 5% and 10% were 71.5% and 71.8% lower than Bionate, respectively. Chronosil 10% became slightly stiffer after the initial compression of Test 1.

Regarding deformation, the tendency for the height was to decrease after Test 1, recover a proportion after 24 hours (but not fully recovery, demonstrating that plastic deformation occurred) and decrease again after Test 2 by a smaller percentage in comparison with Test 1 (indicating that the material became stiffer after the first compression). This behaviour was seen for the materials containing the carbonate group in their composition. Only Elast Eon specimens deformed more in height after the second compression of Test 2 which may be caused by the lack of the carbonate group. Elast Eon samples presented the largest percentage of deformation in all cases (after Test 1, Test 2 and in total) and also recovery (between Test 1 and Test 2) for all dimensions: height, length and width. The total deformation in height accounted for a  $4.1 \pm 0.5\%$  reduction with respect to the original height. Although there was little information regarding Elast-Eon 82A E5-325 composition, the quantity of silicone may be an important factor given the deformations shown in this study. Chronosil 10% also deformed markedly. Chronosil 5% deformed less than Chronosil 10% ( $2.7 \pm 0.3\%$  vs  $3.2 \pm 0.5\%$  of total height deformation), which was expected due to the lower quantity of silicone. Samples of Chronosil 5% followed similar patterns of deformation in comparison with the Chronosil 10% but with lower values. Bionate II 80A presented the smallest percentages of dimensional changes with a total deformation in height of  $1.1 \pm 0.2\%$ . These results were expected given the material composition that includes a hard segment from the polycarbonate group and it excludes the silicone content.

The materials analysed in this study did not demonstrate sufficient stiffness to withstand the loads of the lumbar spine with the specimen dimensions proposed. The size of the implant, and consequently the size of the elastomeric core, was limited by the proposed surgical procedure (Soriano-Baron et al., 2015). The small specimen dimensions may have caused the stiffness values obtained not meeting the stiffness required. This is due to the stiffness being directly proportional to the cross section area of the specimen (Gere and Timoshenko, 1999). However the testing results provided in this paper can guide other researchers on the better application of these materials for other biomedical purposes.

Further development of the device is required to confirm the mechanical and clinical feasibility of the proposed design. Several options could be considered for future work: (1) widening the range of



elastomers used in the implant, particularly pure PCU elastomers, may mean that the stiffness requirements can be met; any other additive would likely weaken the strength properties of the elastomer; (2) another strategy may be to explore further elastomers with shore hardness in excess of the 80A of the current materials in this study; (3) the possibility of exploiting hyper-elasticity to gain increased stiffness could be considered for Bionate II 80A material, the average stiffness of which at 3 mm of displacement was 973.68 N/mm, almost achieving the target stiffness; and (4) further options could involve other mechanisms to provide compression stiffness different than elastomeric cores such as compression springs, elastomeric composites or a combination of both. In vivo studies will be required to assess the clinical feasibility of the final solution.

## 5. CONCLUSION

A novel design of an elastomeric lumbar disc replacement that is implanted via transforaminal approach has been investigated. Several biomaterials have been mechanically tested in compression and the results are presented. Finding an elastomeric material able to withstand the loads of the lumbar spine with the device dimensions restricted by the transforaminal approach continues to be a challenge and further work is required to develop the design proposed.

## ACKNOWLEDGMENTS

The authors would like to thank Johann Robin, Brice Sennequier and Bernard M. Lawless for their assistance in purchasing the biomaterials. This research was supported by the European Commission under the 7th Framework Programme. (Grant agreement no.: 604935).

## REFERENCES

- Abi-Hanna, D., Kerferd, J., Phan, K., Rao, P., & Mobbs, R. (2018). Lumbar disc arthroplasty for degenerative disc disease: a literature review. *World Neurosurgery*, 109, 188-196.
- ASTM International F2346-05. (2011). Standard Test Methods for Static and Dynamic Characterization of Spinal Artificial Discs.
- Auerbach, J. D., Wills, B. P., McIntosh, T. C., & Balderston, R. A. (2007). Evaluation of spinal kinematics following lumbar total disc replacement and circumferential fusion using in vivo fluoroscopy. *Spine*, 32(5), 527-536.
- Baliga, S., Treon, K., & Augus Craig, N. J. (2015). Low Back Pain : Current Surgical Approaches. *Asian Spine Journal*, 9 (4), 645–657.
- Bouzakis, K. D., Mitsi, S., Michailidis, N., Mirisidis, I., Mesomeris, G., Maliaris, G., ... & Anagnostidis, K. (2004). Loading simulation of lumbar spine vertebrae during a compression test using the finite elements method and trabecular bone strength properties, determined by means of nanoindentations. *Journal of Musculoskeletal and Neuronal Interactions* 4(2), 152-158

- British Standards Institution (2011). BS ISO 18192-1:2011 Implants for Surgery. Wear of total intervertebral spinal disc prostheses. Part 1: Loading and displacement parameters for wear testing and corresponding environmental conditions for test.
- Deng, Q., Ou, Y., Zhu, Y., Zhao, Z., Liu, B., Huang, Q., ... Jiang, D. (2016). Clinical outcomes of two types of cages used in transforaminal lumbar interbody fusion for the treatment of degenerative lumbar diseases: n-HA / PA66 cages versus PEEK cages. *Journal of Materials Science: Materials in Medicine*, 27(6), 1–9.
- Eckold, D. G., Dearn, K. D., & Shepherd, D. E. T. (2015). The evolution of polymer wear debris from total disc arthroplasty. *Biotribology*, 1, 42-50.
- Francolini, I., & Piozzi, A. (2016). Antimicrobial polyurethanes for intravascular medical devices. In book: *Advances in Polyurethane Biomaterials*, 349-385. Elsevier Inc.
- Gardner-Morse, M. G., & Stokes, I. A. (2004). Structural behavior of human lumbar spinal motion segments. *Journal of Biomechanics*, 37(2), 205-212.
- Gere, J. M., & Timoshenko, S. (1999). Mechanics of Materials. 4th SI. Cheltenham: *Stanley Thornes*.
- Gunatillake T. & Adhikari R. (2016) Nondegradable synthetic polymers for medical devices and implants. In book: *Biosynthetic Polymers for Medical Applications*, 33-62. Woodhead Publishing.
- Han, S., Hyun, S. J., Kim, K. J., Jahng, T. A., & Kim, H. J. (2017). Comparative study between cobalt chrome and titanium alloy rods for multilevel spinal fusion: proximal junctional kyphosis more frequently occurred in patients having cobalt chrome rods. *World neurosurgery*, 103, 404-409.
- Inoue, N., & Orías, A. A. E. (2011). Biomechanics of intervertebral disk degeneration. *Orthopedic Clinics of North America*, 42(4), 487-499.
- John, K. R. S. (2014). The use of polyurethane materials in the surgery of the spine: a review. *The Spine Journal*, 14(12), 3038-3047.
- Kemper, A. R., McNally, C., & Duma, S. M. (2007). The influence of strain rate on the compressive stiffness properties of human lumbar intervertebral discs. *Biomedical Sciences Instrumentation*, 43, 176-181.
- Klues, D., Mittelmeier, W., & Bader, R. (2010). Intraoperative impaction of total knee replacements: An explicit finite-element-analysis of principal stresses in ceramic vs. cobalt–chromium femoral components. *Clinical Biomechanics*, 25(10), 1018-1024.
- Lawless, B. M., Barnes, S. C., Espino, D. M., & Shepherd, D. E. (2016). Viscoelastic properties of a spinal posterior dynamic stabilisation device. *Journal of the Mechanical Behavior of Biomedical Materials*, 59, 519-526.
- Lazennec, J. Y., Aaron, A., Brusson, A., Rakover, J. P., & Rousseau, M. A. (2013). The LP-ESP® lumbar disc prosthesis with 6 degrees of freedom: development and 7 years of clinical experience. *European Journal of Orthopaedic Surgery and Traumatology*, 23(2), 131-143.
- Okoro, T., & Sell, P. (2010). A short report comparing outcomes between L4/L5 and L5/S1 single-level discectomy surgery. *Clinical Spine Surgery*, 23(1), 40-42.

- Osman, A. F., Edwards, G. A., Schiller, T. L., Andriani, Y., Jack, K. S., Morrow, I. C., ... & Martin, D. J. (2011). Structure–property relationships in biomedical thermoplastic polyurethane nanocomposites. *Macromolecules*, 45(1), 198-210.
- Panjabi, M. M., Oxland, T. R., Yamamoto, I., & Crisco, J. J. (1994). Mechanical behavior of the human lumbar and lumbosacral spine as shown by three-dimensional load-displacement curves. *Journal of Bone and Joint Surgery*, 76(3), 413-424.
- Park, C. K. (2015). Total disc replacement in lumbar degenerative disc diseases. *Journal of Korean Neurosurgical Society*, 58(5), 401.
- Rao, M. J., & Cao, S. S. (2014). Artificial total disc replacement versus fusion for lumbar degenerative disc disease: a meta-analysis of randomized controlled trials. *Archives of Orthopaedic and Trauma Surgery*, 134(2), 149-158.
- Salzmann, S. N., Plais, N., Shue, J., & Girardi, F. P. (2017). Lumbar disc replacement surgery—successes and obstacles to widespread adoption. *Current Reviews in Musculoskeletal Medicine*, 10(2), 153-159.
- Soriano-Baron, H., Newcomb, A. G., Malhotra, D., de Tranaltes, K., Martinez-del-Campo, E., Reyes, P. M., ... & Tumialán, L. M. (2015). Biomechanics of Nested Transforaminal Lumbar Interbody Cages. *Neurosurgery*, 78(2), 297-304.
- Vicars, R., Hall, R., & Hyde, P.J. (2017). 7.14 Wear : Total Intervertebral Disc Prostheses. *Comprehensive Biomaterials II*. 246-264
- Virgin, W. J. (1951). Experimental investigations into the physical properties of the intervertebral disc. *Bone and Joint Journal*, 33(4), 607-611.
- Vital, J. M., & Boissière, L. (2014). Total disc replacement. *Orthopaedics & Traumatology: Surgery and Research*, 100(1), S1-S14.
- Ward, R., & Jones, R. (2011). Polyurethanes and silicone polyurethane copolymers. In *Comprehensive Biomaterials*. 431-477. Oxford: Elsevier.
- White, A. A., & Panjabi, M. M. (1990). *Clinical Biomechanics of the Spine* (2), 108-112. Philadelphia: Lippincott.
- Yao, C., Lu, J., & Webster, T. J. (2011). Titanium and cobalt–chromium alloys for hips and knees. In *Biomaterials for Artificial Organs* (34-55).
- Zhang, Q., Yuan, Z., Zhou, M., Liu, H., Xu, Y., & Ren, Y. (2014). A comparison of posterior lumbar interbody fusion and transforaminal lumbar interbody fusion: a literature review and meta-analysis. *BMC Musculoskeletal Disorders*, 15(1), 367.